Excerpt from the Proceedings of the 2011 COMSOL Conference in Stuttgart

Stress analysis of an electromagnetic horn with separated target

B Lepers
IPHC, Université de Strasbourg, CNRS/IN2P3, F-67037 Strasbourg, France
benjamin.lepers@gmail.com

September 5, 2011

Abstract

A electromagnetic horn is a device positioned around a target and used to focus charged particles toward a detector with a strong pulsed toroidal magnetic field. In the framework of the European Euronu project for the next neutrino factory facility, a 4 MW protons beam will be distributed in 4 horn/target system.

Current density, magnetic flux and resistive loss distributions are obtained for the horn with non integrated target by solving Maxwell's Ampere law equation for a time harmonic current excitation. The temperature field is then obtained by solving the heat conduction equation for two cooling scenario. The total displacement and von mises stress are obtained by solving a transient mechanical model with a magnetic pressure pulse load and with the initial displacement field due to thermal dilatation calculated with a Comsol static thermo mechanical model.

1 Introduction

Simulation of a hadron focusing horn have been made using particle production code such as GEANT or FLUKA and an optimal closed forward geometry with non integrated target has been found for the super beam [1],[2]. In summary, high magnetic field closed to the target and small material thickness are desirable to obtain the best positive muons focusing and minimize secondary particles production [3].

Given the nominal values of the proton beam power $P = 4$ MW and horn peak current $I_0 = 350$ kA, high power density is located inside the target and horn wall conductors. The feasibility of this horn design depends mainly on the temperature and stress level inside the target and horn structure. It has been shown [4] that the integrated target/horn required very high cooling, and may have a reduced lifetime. The new baseline design is a target with its own cooling system and separated to the horn.

In working condition, the horn will be in thermal equilibrium with its environment and the cooling system will be design to limit the maximal temperature of the Aluminium alloy to $60°C$. h convection coefficients required to maintain this temperature can be calculated by heat flux conservation for each horn segments. The displacements and stress distribution due to thermal dilatation are given by the static coupled electro thermo mechanical model.

The pulsed magnetic field creates a periodic magnetic pressure pulse on the horn wall. The total displacement and stress field are the sum of the thermal static field and the transient field due to magnetic pulses. For the transient part, the total displacement and stress field is obtained by solving a transient mechanical model over one pulse with the initial conditions being the initial deformation due to thermal dilatation.

This study presents the electrical, thermal and mechanical analysis with a finite element model using Comsol 3.3 in steady state and transient regime for the non integrated target horn design.

2 Horn geometry and physics parameters

The horn system with the strip lines and the cooling circuit is shown in figure 1 and dimen-

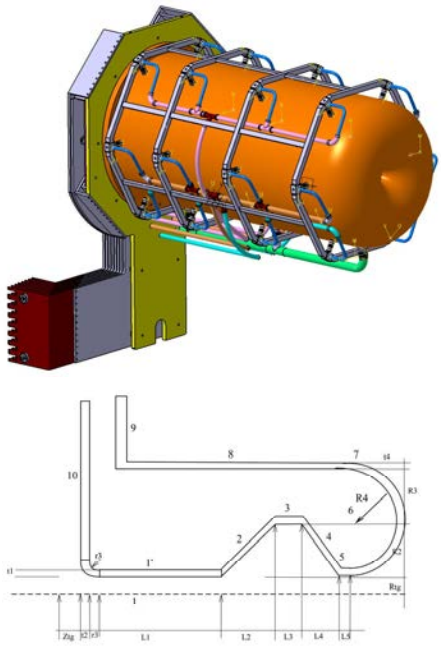

Figure 1: Horn system with striplines and cooling system and 2d schematic

Properties	Aluminium 6061 T6	Glass
Electrical conductivity [S/m] σ		10^{-14}
σ @ $20°C$	2.63×10^7	
σ @ $60°C$	2.27×10^7	
Thermal conductivity [W/(m K)] k	$k(200) = 163$, $k(400) = 186$, $k(600) = 186$	1.38
Thermal expansion coeff $[10^{-6}/K]$ α	24	0.55
Elastic young modulus [GPa] E	70	73.1
poisson coefficient ν	0.33	0.17
Parameters	value [mm]	-
L_1, L_2, L_3, L_4, L_5	589, 468, 603, 475, 10.8	-
t_1, t_2 , t_3, t_4	3, 10, 3, 10	-
r_1, r_2	108	-
r_3	50.8	-
R^{tg}	12	-
L^{tg}	780	-
z^{tg}	68	-
R_2, R_3, R_4	191, 359, 272	-
R_1 non integrated	30	-

Table 1: Thermal properties obtained from references[5] and dimensions .

sions are given in table 1. With a 4 horn scheme, the proton beam will be distributed on the four targets and the repetition frequency for the pulsed current will be 12.5 Hz. In the case of 1 horn failure, the system must be able to continue working with 3 horns giving a power of 1.3 MW per horn.

3 Material properties

Some electrical, thermal and mechanical properties used in the finite element model are given in table 1 for Aluminium and Ceramic Glass. Some properties may vary according to the specific alloy.

The non integrated target will incorporate its own helium cooling circuit and no supplementary heat flux coming from the target will be transfer to the horn. The jet cooling circuit for the horn will have to be design in order to achieve a uniform maximal temperature of $60°C$ everywhere in the horn. This level of working temperature is to maintain good mechanical strength.

4 Electrical part

4.1 Currents and magnetic flux

A strong toroidal magnetic field used to focus the positively charged particles (mainly π^+) in the case of neutrino runs and defocus the negative charged particles π^- (the opposite for anti neutrino runs) toward a decay channel is created by a circulation of a high intensity electrical current. In operation, this high magnetic field is generated by pulsed currents. The pulsed electrical current circulating in the horn has a sinus half period of $\tau_0 = 100\,\mu$s and periodicity of $T = 20$ ms or 80 ms in the case of a 4 horn scheme. The specifications of a horn electrical pulser system are described in [8]. Assuming one horn failure, the frequency for the 3 remaining horns will be $\frac{50}{3} = 16.7\,Hz$ which correspond to a time period of $T = 60\,ms$ between two consecutive pulses. The electrical model uses a sinusoidal current of frequency $f = \frac{1}{200\times10^{-6}} = 5000$ Hz and peak current $\sqrt{2}I_{rms} = 14.3$ kA, $I_{rms} = 10.1$ kA.

For the inner conductor of the horn, most of the current flows between the surface and the

skin depth δ

$$\delta = \sqrt{\frac{2\,\rho_{el}}{\omega\,\mu}} \tag{1}$$

which is about 1.4 mm for Al 6061-T6 with the electrical resistivity $\rho_{el} = 3.8 \times 10^{-8} \Omega\, m$. For the outer conductor of the horn, most of the current flow between the inner radius of the outer conductor and the skin depth.

The magnetic field is maximum when the current is at his peak of $I_0 = 350$ kA for approximately 5 μs. Four domains can be identified to calculate the magnetic field:

- $0 \leq r \leq r_{i1}$, domain 1, $B(r) = 0$: no magnetic field inside the annular space
- $r_{i1} \leq r \leq r_{e1}$, domain 2, $B(r)$: magnetic field inside the inner conductor
- $r_{e1} \leq r \leq r_{i2}$, domain 3, B(r): magnetic field in the horn cavity between the 2 conductors.
- $r_{i2} \leq r \leq r_{e2}$, domain 4, B(r): magnetic field inside the outer conductor.

Assuming constant current density, the current is:

$$J(r) = \begin{cases} 0 & \text{if } 0 < r < r_{i1} \\ J_{01} & \text{if } r_{i1} < r < r_{e1} \\ 0 & \text{if } r_{e1} < r < r_{i2} \\ J_{02} & \text{if } r_{i2} < r < r_{e2} \end{cases}$$

Using Maxwell's equation; the magnetic flux is:

$$B(r) = \begin{cases} 0 & \text{if } 0 < r < r_{i1} \\ \frac{\mu I_0 (r^2 - r_{i1}^2)}{2\pi r (r_{e1}^2 - r_{i1}^2)} & \text{if } r_{i1} < r < r_{e1} \\ \frac{\mu I_0}{2\pi r} & \text{if } r_{e1} < r < r_{i2} \\ \frac{\mu I_0}{2\pi r} - \frac{\mu I_0}{2\pi r} \frac{r^2 - r_{i2}^2}{r_{e2}^2 - r_{i2}^2} & \text{if } r_{i2} < r < r_{e2} \end{cases}$$

The magnetic flux is maximal at the surface of the inner conductor $r_{e1} = 3.3$ cm with $B(0.033) = 2.12$ T.

4.2 Electromagnetic harmonic model

The horn model is a 2 D axisymmetric trapezoidal contour with currents in the r-z plan. The magnetic field has only a H_ϕ component out of the plane. From Maxwell's equation in the frequency domain, we can obtain an equation for the magnetic field:

$$\begin{aligned} \nabla \times \mathbf{E} &= -j\omega\mu\mathbf{H} \\ \nabla \times \mathbf{H} &= (\sigma + j\omega\epsilon)\mathbf{E} \end{aligned} \tag{2}$$

with σ and ϵ the electrical conductivity and electrical permeability of the material. Using equation 2, the equation for the magnetic field is:

$$j\omega\mu\mathbf{H} + (\sigma + j\omega\epsilon)^{-1} \nabla \times [\nabla \times \mathbf{H}] = 0 \tag{3}$$

From axial symmetry, the current density vector is in the r-z plane $\mathbf{J} = J_r \boldsymbol{e_r} + J_z \boldsymbol{e_z}$ and the magnetic field has only an azimuthal component, $\mathbf{H} = H_\phi \boldsymbol{e_\phi}$. Using ampere law with the quasi static assumption ($\lambda >> L$), the current density is calculated from the magnetic field components:

$$\begin{aligned} \mathbf{J} &= \nabla \times \mathbf{H} \\ &= -\frac{\partial H_\phi}{\partial z} \boldsymbol{e_r} + (\frac{H_\phi}{r} + \frac{\partial H_\phi}{\partial r}) \boldsymbol{e_z} \end{aligned} \tag{4}$$

The time average resistive heating is calculated as follows:

$$Q_{av} = \frac{1}{2\sigma} \mathbf{J}\mathbf{J}^* \tag{5}$$

with $\mathbf{J}^*$ the complex phasor conjugate of $\mathbf{J}$ [1]

On the input end plate the circumferential component of the magnetic field is specified:

$$H_\phi = \frac{\sqrt{2} I_{rms}}{2\pi r} \tag{6}$$

[1] For time harmonic fields, the time average of the product of two vectors is:

$$\begin{aligned} \overline{\vec{A}(\mathbf{r},t) \cdot \vec{B}(\mathbf{r},t)} &= \frac{1}{2} Re(\mathbf{A} \cdot \mathbf{B}^*) \\ \vec{A}(\mathbf{r},t) &= Re(\mathbf{A} e^{j\omega + \phi}) \end{aligned}$$

with $\mathbf{A}^*$ is the complex conjugate phasor

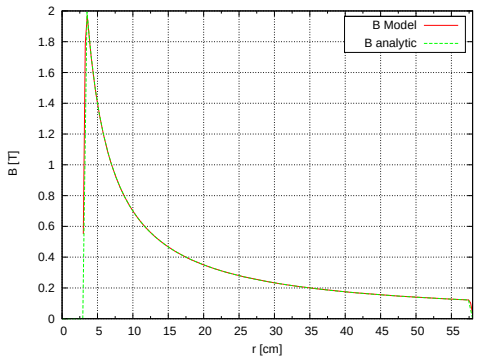

Figure 2: Modelled and analytic radial magnetic flux distribution at $z = 20$ cm with peak current $I = 350$ kA.

This condition assigned the value of the circumferential H_ϕ magnetic field according to Amperes law. Inside the structure, continuity of the electric field is prescribed, for the contour of the geometry, the magnetic field is assumed to be 0, the magnetic insulation is expressed as $\mathbf{n} \times \mathbf{E} = 0 \Leftrightarrow H_n = 0$ with $\mathbf{n}$ the normal vector of the external surfaces of the horn.

4.3 Magnetic flux distribution and resistive loss

In figure 2 are plotted the calculated magnetic flux with constant current density assumption and the calculated magnetic flux using the finite element model and taking into account the current surface effect. Difference exist in distribution only in the inner and outer conductor of the horn, where the current distribution has an effect. According to Amperes law the magnetic flux at a given radius depends on the total current enclosed by the the magnetic contour. The total current is I_0 and its distribution (skin effect or constant) does not affect the magnetic field inside the horn cavity between the 2 conductors as shown in figure 2

Most electrical losses came from the inner conductor, conical sections and top end of the horn as indicated in table 2.

Q[kW]	tot	1+1'	2	3	4	5 + 6	7	8	9	10
$\sigma_{20} = 2.63 \times 10^7 \frac{S}{m}$	21	9.15	2.4	1.2	2.4	2.6	0.39	1.64	0.14	1.0
$\sigma_{60} = 2.27 \times 10^7 \frac{S}{m}$	22.8	10	2.6	1.3	2.6	2.8	0.43	1.77	0.15	1.1
Q_s	38.5	15.1	2.3	1.7	1.2	0.85	0.14	13	0	5.4

Table 2: Resistive loss in each conductor for electrical conductivity at $20°C$ and $60°C$. The conductor number are indicated in figure 1. Power Q_s deposited from secondary particles is indicated in the last row .

5 Thermal static model

In steady state regime the axial-symmetric model is described by the heat conduction equation:

$$\nabla \cdot [k \nabla T(r,z)] + q(r,z) = 0. \qquad (7)$$

The heat source density distribution is composed of:

$$q(r,z) = q_{\text{secondary}}(r,z) + q_{\text{Joule}}(r,z) \qquad (8)$$

$q_{\text{secondary}}(r,z)$ is the energy deposited in the horn from secondary particles calculated with FLUKA, about 38 kW in total. $q_{\text{Joule}}(r,z)$ is the resistive loss from electrical currents, about 20 kW for the horn with $I_{rms} = 10.1$ kA current (i.e 3 horn running scenario). The radiative heat flux coming from the hot target can be neglected in comparison to the convection cooling flux. The total power density is plotted in figure 3 and the resistive power loss and power deposited from secondary particle for each horn segment is given in the table 2.

The boundary conditions are applied as follows. Thermal insulation is specified everywhere on the external wall of the horn. For the internal wall, uniform heat convection is applied to simulate the cooling characterised by an average heat transfer coefficient $\{h_{horn}, h_{inner}\} = \{1, 1\}$ kW/(m^{2}K). This cooling range is achievable with water sprays distributed along the outer conductor of the horn and pointing toward the inner conductor. In the circumferential direction, a design of 6 jets equally spaced covering an angle of $60\,°C$ is chosen. As show in figure 4, the inner conductor needs more active cooling. Based on energy conservation it is possible to

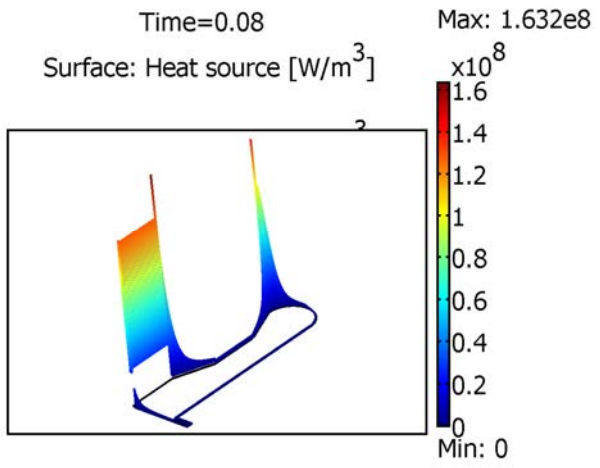

Figure 3: Total power density distribution

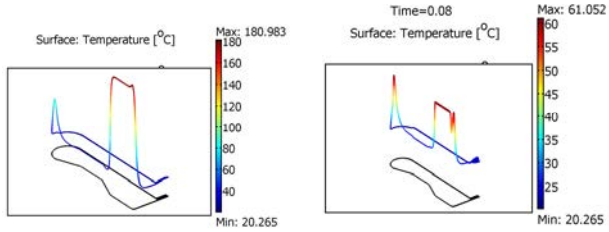

a) b)

Figure 4: Temperature field, max temperature around $180\,^{\circ}C$, for the cooling scenario $\{h_{inner}, h_{horn}\} = \{1, 1\}$ kW/(m^{2}K) fig a); max temperature of $61\,^{\circ}C$ for $\{h_{inner}, h_{horn}, h_{corner}, h_{conv}\} = \{3.8, 1, 6.5, 0.1\}$ kW/(m^{2}K) fig b)

calculate for each horn segments, the minimum h coefficient to maintain a uniform horn temperature of $60\,^{\circ}C$. The radiative heat flux coming from the hot target can be neglected in comparison to the convection cooling flux.

The temperature distribution is plotted in figure 4 for a basic cooling scenario of $\{h_{inner}, h_{horn}\} = \{1, 1\}$ kW/(m^{2}K) and for an optimized cooling scenario with higher cooling in the hot spot area $\{h_{inner}, h_{corner}, h_{conv}\} = \{3.8, 6.5, 0.1\}$ kW/(m^{2}K). h_{inner}, h_{corner}, h_{conv} being the heat transfer coefficient on the surface of the inner conductor, on the upstream bottom corner (near the target) and on the right side of the upstream bottom plate.

For the uniform cooling, the maximal temperature is $180\,^{\circ}C$. When higher cooling is used in the hot spot area, the maximal temperature is $61\,^{\circ}C$. The water jet nozzles disposition and individual flow rates of the jets will have to be chosen to maintain a reasonable maximal temperature around $60\,^{\circ}C$. This thermal model shows that the two hot area are the upstream bottom corner and the downstream part where the inner radius is $r = 3$ cm.

6 Mechanical static model

In order to assess the horn deformation and horn lifetime, the calculation of the stress inside the horn structure is necessary. The stress level in the structure should be low enough in comparison with the fatigue limit of the materials. After few seconds, the magnetic horn reach steady state temperature with maximal value of $60\,^{\circ}C$ with appropriate cooling. In this section the displacement and thermal stress due to thermal expansion are calculated.

6.1 Material model

For the axial symmetric model, from symmetry of revolution there is no displacement in the circumferential direction $\mathbf{e}_\theta$. In cylindrical coordinates and for small displacements, the strain displacements relationships are:

$$\boldsymbol{\epsilon} = \begin{pmatrix} \epsilon_r \\ \epsilon_\theta \\ \epsilon_z \\ \epsilon_{rz} \end{pmatrix} = \begin{pmatrix} \frac{\partial u_r}{\partial r} \\ \frac{u_r}{r} \\ \frac{\partial u_z}{\partial z} \\ \frac{\partial u_r}{\partial z} + \frac{u_z}{\partial r} \end{pmatrix} \tag{9}$$

Using a linear isotropic elastic model, the stress strain relationships are:

$$\boldsymbol{\sigma} = \mathbf{D}\boldsymbol{\epsilon} \tag{10}$$

with σ and ϵ the stress and strain vectors. and

$$\mathbf{D} = \frac{E}{(1+\nu)(1-2\nu)} \begin{pmatrix} 1-\nu & \nu & \nu & 0 \\ \nu & 1-\nu & \nu & 0 \\ \nu & \nu & 1-\nu & 0 \\ 0 & 0 & 0 & \frac{1-2\nu}{2} \end{pmatrix}$$

E is the module of elasticity or young modulus and ν the Poisson's ratio. The deformation is only due to the thermal dilatation:

$$\boldsymbol{\epsilon} = \boldsymbol{\epsilon_{th}} \tag{11}$$

$$\boldsymbol{\epsilon_{th}} = \begin{pmatrix} \epsilon_r \\ \epsilon_\theta \\ \epsilon_z \\ \epsilon_{rz} \end{pmatrix} = (T - T_{ref}) \begin{pmatrix} \alpha \\ \alpha \\ \alpha \\ 0 \end{pmatrix}$$

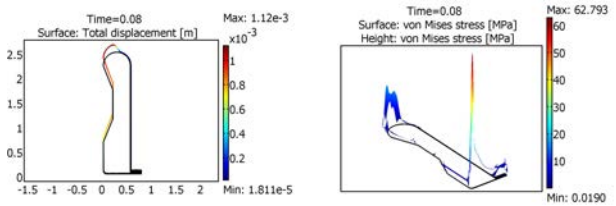

a) b)

Figure 5: Displacement and stress field due to thermal dilatation when the horn is running in steady state regime with a maximal temperature around 60 °C, $u_{max} = 1.12$ mmn $S_{max} = 62$ MPa

α is the coefficient of thermal expansion, T_{ref} is the initial temperature and T is the final temperature, when the horn structure reached thermal equilibrium. Equation of equilibrium for the 2D axisymmetric model are given below:

$$\frac{\partial \sigma_r}{\partial r} + \frac{\partial \tau_{rz}}{\partial z} + \frac{\sigma_r - \sigma_\theta}{r} + F_r = 0 \qquad (12)$$
$$\frac{\partial \tau_{rz}}{\partial r} + \frac{\partial \sigma_z}{\partial z} + \frac{\tau_{rz}}{r} + F_z = 0$$

with $F_r = F_z = 0$ the volume force components. In this analysis, there is no volume forces, the displacement and internal stress are only due to thermal gradients.

6.2 Boundary conditions

The model is axisymmetry and the z displacement of the back plate is fixed to 0.

6.3 Results

The displacement field is plotted in figure 5 a) with a maximal displacement of $u_{max} = 1.12$ mm occurring in the downstream part of the horn (opposite to the target side).

As shown in figure 5 b) the maximal stress of 62 MPa occurs in the corner region. This value is well below the aluminium maximal strength but still high in comparison of Al 6061 T6 fatigue limit for 10^8 cycle. There is also a high stress level in the top inner waist of the horn. This part and segments junctions should required some slight modification to achieve a stress as low as possible below 20 MPa for example.

7 Mechanical transient model

The equations are the equations of equilibrium of section 6.1 except that the strain, stress and loads are function of time.

$$\begin{aligned} \sigma(t) &= \mathbf{D}\epsilon(t) \qquad (13) \\ p(t) &= \frac{\mu i(t)^2}{8\pi^2 r^2} \end{aligned}$$

and

$$i(t) = \begin{cases} I_0 sin(\pi \frac{t}{\tau}) & \text{if } T - \frac{\tau}{2} < t < T + \frac{\tau}{2} \\ 0 & \text{elsewhere} \end{cases} \qquad (14)$$

with $i(t)$ and $p(t)$ the pulsed current and magnetic pressure. $\tau = 100\,\mu s$ is the pulse width and $T = 80\,ms$ is the time period between 2 current pulses. The table 3 summarize the coupled static and transient model with the equations, boundary conditions input and output data. The magnetic pressure pulse is a sinus pulse and the peak magnetic field occurs at time $t = 80\,ms$. The time steps are $t = \{79.95, 79.96, ..., 8.05\}\,ms$ with 0.01 s increment.

The transient stress from the magnetic pressure pulse is significant mainly for the inner conductors of the horn with small radius such as the inner conductor parallel to the target and inner waist in the downstream region. (light blue in figure 7 b) at the maximal magnetic pressure $t = 80\,ms$). The displacement and von mises stress distribution for the horn are given in figure 6.

In figure 7 a) and b) the total displacement $u = \sqrt{u_r^2 + u_z^2}$ and von mises stress is plotted for the conductors segments of the horn. The displacement is maximum in the top part of the horn (dowstream region) as shown by the ligth blue curve for conductor 5. The displacement due to the magnetic pulse is quite low in comparison to the thermal dilatation. The von mises stress is the highest in the upstream corner region. The magnetic pressure pulse contributes of about 20 MPa in the top part of the horn region with $r = 3$ cm.

In figure 7 c) is plotted each stress components at the point $\{r, z\} = \{3.2, 20\}$ located in the inner conductor horn. The thermal dilatation does not contributed to the radial stress but mainly to the longitudinal stress S_z as expected. The thermal static von mises stress is about 2.5 MPa and the peak stress is 16 MPa. Because the inner conductor thickness $e = 3$ mm is small compared to the inner radius $r_i = 30$ mm the hoop stress inside the inner conductor is approximately constant and is related to the pressure

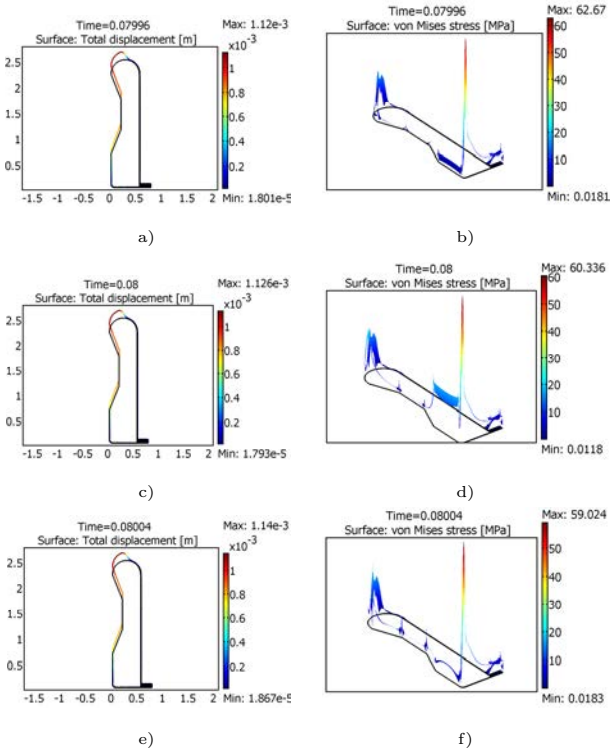

Figure 6: Displacement and stress field due to thermal dilatation and magnetic pulse, $u_{max} = \{1.12, 1.12, 1.14\}$ mm, $S_{max} = \{62.6, 60.3, 59\}$ MPa at time $t = \{79.96, 80, 80.04\}$ ms

by:

$$\begin{aligned} \sigma_{phi} &= \frac{p(r_e)(r_i + e)}{e} \\ &= 18 \times \frac{0.033}{0.003} \\ &\simeq 19\, Mpa \end{aligned} \tag{15}$$

The green line in figure 7 c) shows that the hoop stress is about -19 Mpa, in agreement with the previous analytic calculation (equation 15).

For the euronu horn cern prototype, according to the design report [10] a maximal value of 68 MPa for the 10^8 cycles fatigue limit was used (with a 97.5% confidence). Following industrial standards and the reference [9] the design fatigue curves of Aluminium 6061-T6 show that the maximal fatigue strength limit are $\{50, 20\}$ MPa for 10^8 cycles for zero and with a maximum mean stress respectively.

For the inner conductor horn, the magnetic pressure pulse creates a pic von mises stress of about 16 MPa. This value is below the 20 MPa limit strength for 10^8 cycles with a mean stress due to thermal dilatation.

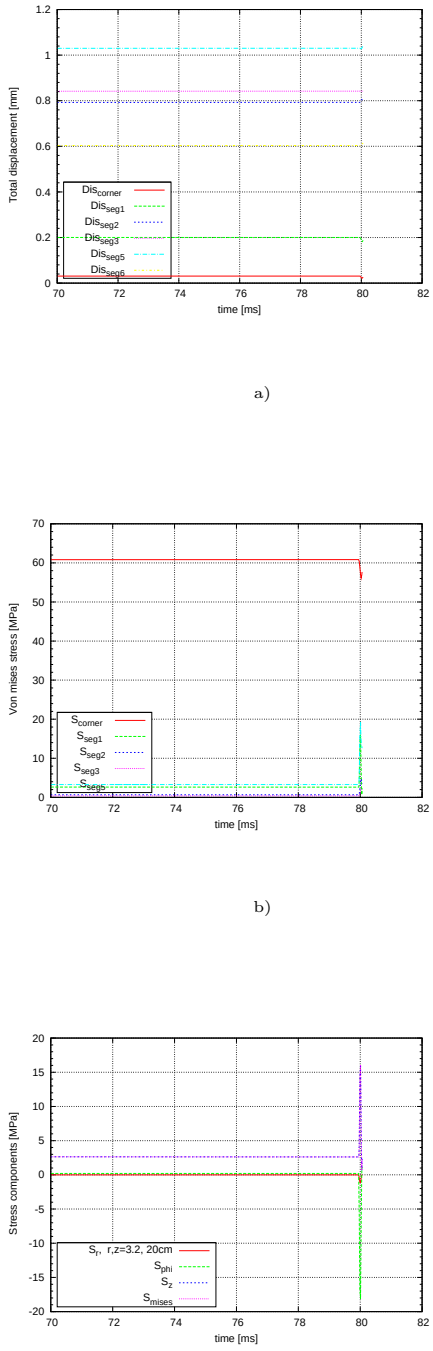

Figure 7: Displacement a) and stress b) due to thermal dilatation and magnetic pulse. Corner $\{r, z\} = \{(6.6, 6.5)\}$ and conductor segments 1, 2, 3, 5, 6 $\{r, z\} = \{(3.2, 20), (15, 100), (22.3, 148.6), (3.2, 225.8), (30.5, 254.1)\}$ cm. The origin is located at 6.8 cm upstream from the inner back plate. Stress components inside the inner conductor, $\{r, z\} = \{3.2, 20\}$ cm c)

Model	Equation	Input	BC	Output
AC	$j\omega\mu\mathbf{H} + \frac{1}{\sigma+j\omega\epsilon}\nabla \times [\nabla \times \mathbf{H}] = 0$ $\sigma_{60} = 2.27 \times 10^7 \frac{S}{m}$	$H_{0\phi} = \frac{\sqrt{2}I_{rms}}{2\pi r}$	$\mathbf{n} \times \mathbf{E} = 0 \Leftrightarrow H_n = 0$	$\mathbf{J}, \mathbf{B}$ Q_{av}
Ther	$\nabla \cdot [k \nabla T] + q = 0$ $k = k(T)$	$q = Q_{beam} + Q_{av}$	$q'' = \bar{h}[T - T_\infty]$	T
Ther Mech linear elast	$\frac{\partial \sigma_r}{\partial r} + \frac{\partial \tau_{rz}}{\partial z} + \frac{\sigma_r - \sigma_\theta}{r} + F_r = 0$ $\frac{\partial \tau_{rz}}{\partial r} + \frac{\partial \sigma_z}{\partial z} + \frac{\tau_{rz}}{r} + F_z = 0$ $\vec{\sigma} = \mathbf{E}\vec{\epsilon}$ $\vec{\epsilon} = \epsilon_{\vec{th}}$ $\epsilon_{\vec{th}} = \mathbf{I}\alpha(T - T_{ref})$	$dF_r = 0$ $dF_z = 0$ α, T	$u_{bc}(z = 0) = 0$	$\mathbf{u}$ $\mathbf{s}$
Trans mech	$\epsilon(t)$, $\sigma(t)$ $\epsilon_{\vec{th}} = \mathbf{I}\alpha(T - T_{ref})$	$\mathbf{u_{tot}}(t = 0) = \mathbf{u}$ $p(r,t) = \frac{\mu i(t)^2}{8\pi^2 r^2}$	idem	$\mathbf{u_{tot}}(t)$ $\mathbf{s_{tot}}(t)$

Table 3: Electrical, thermal and mechanical model.

8 Conclusion

This 2d axisymmetry coupled electrical/thermal/mechanical model in steady state regime allows us to determine first the temperature field and the requirement for the h cooling coefficient. This will determine the water jet cooling system design with the flow rate and the number of jets. Then the stress distribution due to thermal dilatation shows that the stress amplitude is relatively low except in the corner region and top inner waist region where the stress is significant with 60 MPa. The total stress is calculated by taking into account the transient magnetic pulse pressure. The contribution to the magnetic pressure is relatively low except in the region of the horn with $r = 3$ cm. For the inner conductor, the peak dynamic stress is about 15 MPa and 20 MPa in the downstream region. According to design fatigue curves of Aluminium 6061-T6, the maximal fatigue strength in presence of a mean stress (60 MPa for the inner waist region) should not exceed 20 MPa for high number of cycles higher than 10^7 cycles. Finally in the conductors junctions, stress concentrations occur and round corner or thicker connection should be used to avoid failure by crack initiation and propagation.

References

[1] A. Longhin, "A new design for the CERN Frejus neutrino Super Beam" EUROnu WP2-10-04.

[2] C. Bobeth and A. Longhin "Optimisation of hadron focusing for the SPL-Frejus Super Beam" EUROnu WP2-10-02, 2010.

[3] S. Meer " A directive device for charged particle and its use in an enhanced neutrino beam" CERN, 1962

[4] B. Lepers, " Static stress analysis in a forward closed horn with integrated target " EUROnu WP2-10-05

[5] F. Incropera and D. Dewitt, "Fundamentals of heat and mass transfer," School of mechanical engineering Purdue University, John Wiley and Sons, 1996, App A, p.827.

[6] C. Bathias "There is no infinite fatigue life in metallic material" Laboratoire de mecanique de la rupture CNAM/ITMA.

[7] S. Gilardoni "Sudy of particle production and capture for a neutrino facto" CERN-thesis-2004-046

[8] S. Gilardoni *et al* "Updating of short specification of a horn pulser system for a neutrino factor" CERN Nufact Note 129, 2003

[9] G. T. Yahr " Fatigue design curves for 6061-T6 Aluminium " Oak Ridge National Laboratory.

[10] I. Stancu *et al " Technical design report for the MiniBooNE neutrino beam ", 2001*